Bull Earthquake Eng (2012) 10:863–893
DOI 10.1007/s10518-011-9331-x

ORIGINAL RESEARCH PAPER

Shaking table study and modelling of seismic behaviour of confined AAC masonry buildings

Miha Tomaževič · Matija Gams

Received: 22 April 2011 / Accepted: 10 November 2011 / Published online: 20 November 2011

Abstract The response of autoclaved aerated concrete confined masonry buildings to seismic ground motion has been studied. Three 1:4 scale models of residential buildings with the same distribution of walls in plan but different types of floors and number of stories have been tested on a uni-directional shaking table. Lightweight prefabricated slabs have been installed in the case of the three-storey model M1, whereas reinforced concrete slabs have been constructed in the case of three-storey model M2 and four-storey model M3. Model M1 was subjected to seismic excitation along the axis of symmetry, whereas models M2 and M3 were tested orthogonal to it. Typical storey mechanism, characterised by diagonal shear failure mode of walls in the ground floor in the direction of excitation has been observed in all cases. Taking into consideration the observed behaviour, a numerical model with concentrated masses and storey hysteretic rules has been used to simulate the observed behaviour. Storey resistance curves calculated by a push-over method and hysteretic rules, which take into account damage and energy based stiffness degradation hysteretic rules, have been used to model the non-linear behaviour of the structure. Good agreement between the experimentally observed and calculated non-linear behaviour has been obtained.

Keywords Confined masonry · Shaking table test · Aerated autoclaved concrete · Seismic resistance · Modelling of seismic behaviour

1 Introduction

Because of low thermal conductivity and high fire resistance, low weight and acceptable, though low mechanical resistance, autoclaved aerated concrete (AAC) is becoming popular construction material in seismic regions. Although vertical load bearing capacity of AAC is limited because of material's low compressive strength, adequate behaviour of AAC buildings has been observed during recent earthquakes in Greece and Slovenia (Fig. 1). Whereas at least basic experimental research to determine the properties of AAC masonry, needed for

M. Tomaževič (✉) · M. Gams
Slovenian National Building and Civil Engineering Institute, Dimičeva 12, 1000 Ljubljana, Slovenia
e-mail: miha.tomazevic@zag.si

Fig. 1 Confined AAC masonry house in Bovec, Slovenia, resisted M = 4.7 earthquake in 2004 (PGA 0.47 g in the vicinity) without damage (photo by U. Klemen)

seismic resistance verification has been already carried out (Manual 2004; Tanner et al. 2005; Schöps and Jäger 2009; Costa et al. 2011), information regarding the dynamic response of buildings to seismic ground motion and failure mechanism of AAC masonry buildings is still lacking.

With regard to traditional clay and concrete block masonry construction, the dynamic response and failure mechanisms might be different. Low mass density of AAC results in lower inertia forces during earthquakes than in the case of buildings of the same size, made of traditional masonry. In addition, tensile/compressive strength ratio, which influences failure mechanisms, is higher in the case of AAC than in the case of clay and concrete block masonry. As regards the structural system of AAC buildings, prefabricated floors have been developed, which are not in complete compliance with the requirements of the codes, and minimalised cross-sections of vertical confining elements to reduce the thermal bridge effects have been proposed. To better understand the seismic behaviour of such buildings, the producer of AAC material in Slovenia financed the experimental research program, within the framework of which three models of representative buildings have been recently tested on a unidirectional shaking table at Slovenian National Building and Civil Engineering Institute, ZAG, in Ljubljana (Tomaževič and Gams 2010). In this article, the experiments will be briefly presented and the main experimental results discussed.

2 Prototype buildings and materials

The prototypes of the tested models represented typical AAC confined masonry buildings, built in the region (Fig. 2). Since the size of the models in plan was adjusted to the dimen-

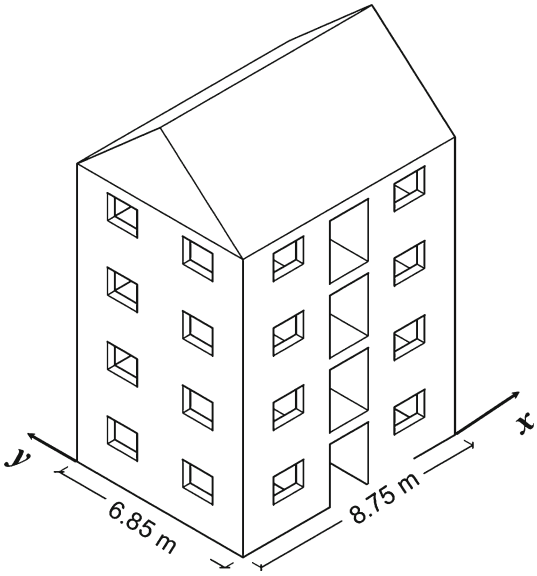

Fig. 2 Axonometric view of the four-storey prototype building

sions of shaking table, the models represented only part of the actual buildings, keeping however the same all important structural characteristics of typical confined AAC buildings. Consequently, imaginary prototype buildings are 6.85 m by 8.75 m in plan, with clear storey height equal to 2.50 m. Wall/floor area ratio is 5.8% in the direction of x-axis (long, weak axis) and 8.3% in the direction of y-axis (short, strong axis = axis of symmetry). The walls are 30 cm thick and are built with AAC masonry units with dimensions 62.5/25/30 cm (length/height/thickness) in thin layer mortar (glue). The distribution of walls in plan is shown in Fig. 3. Two different types of floors are used in prototype construction: 20 cm thick floor system consisting of prefabricated joists, cross-beams and AAC filler blocks, and 15 cm thick monolithic reinforced concrete slabs. The confining tie-columns are located as required by EC 8 (CEN 2004) at all corners and wall intersections, as well as at the ends of openings larger than 1.5 m^2. Tie-columns in confined AAC buildings are of circular section, 16 cm in diameter, reinforced with 4 Ø 14 mm bars, or 10 cm in diameter, reinforced with 4 Ø 16 mm bars. Reinforcing steel of class S440 (yield stress 440 MPa) and concrete of class C25/30 are used. All buildings have horizontal confining r.c. bond-beams at the top of the walls. The main characteristics of the tested prototype buildings are presented in Table 1.

Although minimum units' strength 5 MPa is recommended for the construction of buildings in seismic zones by Eurocode 8, AAC units are traditionally produced in strength classes 2, 4 and 6 MPa. Mechanical properties of units and masonry, corresponding to each strength class of AAC, as given in design manual (Ytong Manual 2004), are summarized in Table 2. As the available data indicate, compressive strength of strength class 4 AAC units complies with the minimum requirements of Eurocode for the use of units in structural walls ($f_{b,P} = 5$ MPa).

The meaning of symbols in Table 2 is as follows:

γ_P mass density of prototype masonry,
$f_{b,P}$ nominal compressive strength of prototype units,
$f_{c,P}$ average compressive strength of prototype masonry,

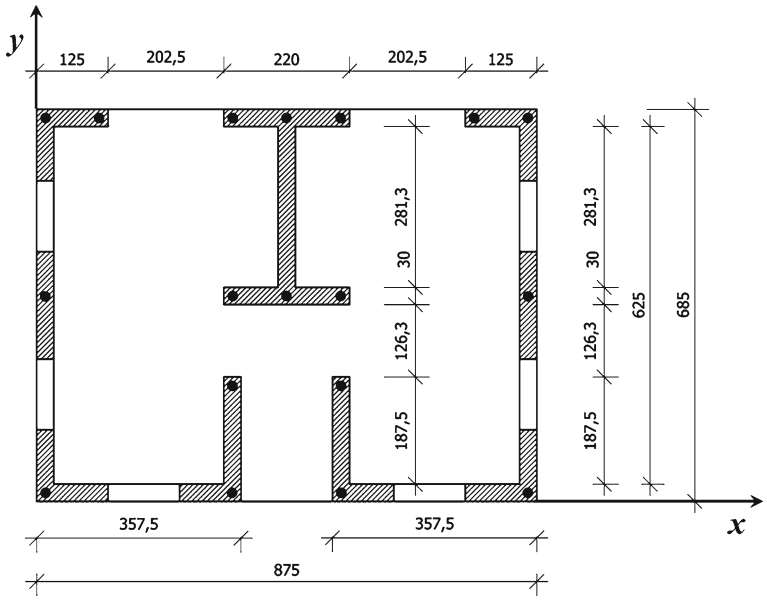

Fig. 3 Floor plan of the prototype building with marked positions of tie-columns

Table 1 Prototype buildings' characteristics

Represented by	Model M1	Model M2	Model M3
Number of storeys	3 + attic	3 + attic	4 + attic
Floor system	Prefabricated	R.c. slabs	R.c. slabs
Tie-column diameter	16 cm	16 cm	10 cm
Direction of loading	y	x	x

Table 2 Mechanical properties of AAC units and masonry (Ytong Manual 2004)

Strength class	γ_P (kg m^{-3})	$f_{b,P}$ (MPa)	$f_{c,P}$ (MPa)	$f_{td,P}$ (MPa)	E_P (MPa)	G_P (MPa)
2	440	2.5	2.14	0.22	1,200	480
4	500	5.0	3.92[a]	0.24[a]	2,200[a]	880[a]
6	660	7.5	5.35	0.26	3,000	1,200

[a] Interpolated values

$f_{td,P}$ average diagonal tensile strength of prototype masonry with thin mortar in bed and head joints, obtained by diagonal compression tests,
E_P modulus of elasticity of prototype masonry,
G_P shear modulus of prototype masonry.

When analyzing the values of mechanical properties, given in Table 2, it can be seen that the values of diagonal tensile strength of AAC masonry, which is critical for shear resistance of masonry walls, do not vary significantly with the increased compressive strength of AAC.While the compressive strength of masonry built of class 6 units is 5.35/2.14 = 2.50-

times greater than compressive strength of masonry built of class 2 units, the increase in diagonal strength is only 18%.

3 Design of models, model materials and selection of seismic loading

3.1 General

When studying the non-linear seismic behaviour of masonry buildings by testing their models on seismic simulators, two basic conditions should be fulfilled:

- the distribution of masses and stiffnesses along the height of the model and prototype should be similar (similitude in dynamic behaviour);
- the working stress in masonry walls/compressive strength of masonry ratio in the case of the model and prototype walls should be similar (similitude in failure mechanisms).

If both conditions are fulfilled, the seismic response and failure mechanisms of prototype and model will be similar to make possible the conversion of values of physical quantities, measured on the model, to the prototype in accordance with similitude laws. If a general physical quantity is measured on the model, q_M, a correlation between the corresponding quantity on the prototype, q_P, is defined by Langhaar (1951), Tomaževič and Velechovsky (1992), Harris and Sabnis (1999):

$$q_P = q_M S_q, \tag{1}$$

where S_q is the scale factor for a given physical quantity. The relationships between physical quantities measured on the model and prototype values depend on the scale of the model and properties of model materials. In the case of the so called general model similitude, the scale factors for the transformation of basic quantities are given in Table 3.

The relationships are simpler in the case of the so called complete similitude (true model), in the case of which the strength properties of material are reduced at geometry scale, whereas some other characteristics, such as strain, specific mass and material damping remain the same as in the case of the prototype. To utilise the capacity of earthquake simulator in the particular case studied, the models have been built at 1:4 scale. When studying the

Table 3 Scale factors in the case of general model similitude

Physical quantity	Scale factor
Length (l)	$S_L = l_P/l_M$
Strength (f)	$S_f = f_P/f_M$
Strain (ε)	$S_\varepsilon = \varepsilon_P/\varepsilon_M$
Specific weight (γ)	$S_\gamma = \gamma_P/\gamma_M$
Displacement (d)	$S_d = S_L$
Force (F)	$S_F = S_L^2 S_f$
Time (t)	$S_t = S_L(S_\varepsilon S_\gamma/S_f)^{0.5}$
Frequancy (ω)	$S_\omega = 1/S_t$
Velocity (v)	$S_v = (S_\varepsilon S_f/S_\gamma)^{0.5}$
Acceleration (a)	$S_a = S_f \ /(S_L S_\gamma)$

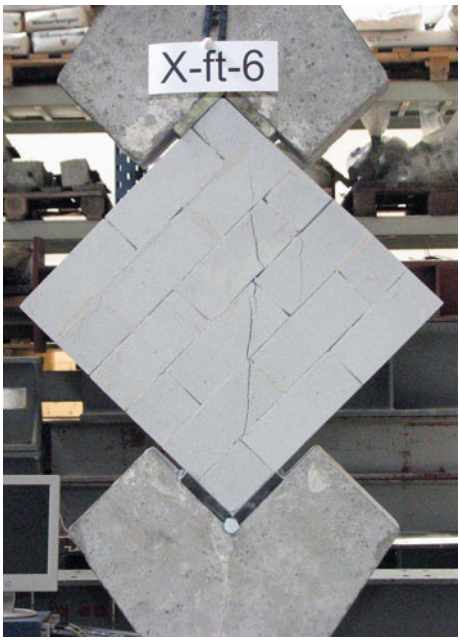

Fig. 4 Diagonal compression test of a model masonry wall

possibilities of producing model AAC material with characteristics, fulfilling the requirements of complete modelling at the same scale, it has been found that, by reducing the strength, the time needed for hardening of AAC is excessively increased. After several trials, a compromise has been made and materials not completely fulfilling the requirements for complete modelling, have been used for the construction of models. The non-compliances with the rules of the complete model similitude, however, have been taken into consideration when evaluating the test results to the prototypes. The issue will be discussed later.

3.2 Model materials

15.6/6.3/7.5 cm (length/height/thickness) model masonry units have been produced in the factory. When needed, special tools have been used to adjust their dimensions during the construction of models in the laboratory. The units have been bonded together with the same factory made thin layer mortar (glue) as in the case of construction of prototype buildings. Compressive strength of units was determined on cubes 6.3/6.3/6.3 cm, cut from the units, whereas compressive strength and modulus of elasticity of masonry have been determined on model walls with dimensions 46.9/68.8/7.5 cm (length/height/thickness). Diagonal tensile strength of masonry was determined by testing model walls at diagonal compression ($f_{td,M}$, Fig. 4). Experimentally obtained values of mechanical characteristics of model masonry are compared with prototype values in Table 4. The values of AAC strength class 4 units (block strength 5 MPa) and masonry, given in Table 2, have been considered as target prototype values. The values of target prototype/actual model ratios are compared with respective scale factors for the case of complete model similitude.

Table 4 Strength characteristics of model masonry and comparison with prototype values for masonry made of strength class 4 AAC masonry units

γ_M (kg m^{-3})	γ_P/γ_M	S_γ (MPa)	$f_{b,M}$	$f_{b,P}/f_{b,M}$ (MPa)	S_f	$f_{c,M}$	$f_{c,P}/f_{c,M}$ (MPa)	S_f	$f_{td,M}$	$f_{td,P}/f_{td,M}$	S_f
496	1.0	1.0	1.59	3.14	4.0	1.49	2.63	4.0	0.25	0.96	4.0

The meaning of symbols in Table 4 is as follows:

γ_M mass density of model masonry,
$f_{b,M}$ average compressive strength of model units,
$f_{c,M}$ average compressive strength of model masonry,
$f_{td,M}$ average diagonal tensile strength of model masonry, obtained by diagonal compression tests.
S_γ, S_f mass density and strength scale factors, respectively, for the case of complete model.

As can be seen, reasonably good agreement between the target and actually obtained values has been obtained for mechanical properties in compression. The tensile strength of model masonry, however, obtained by diagonal compression tests (Fig. 4), was practically the same as that of the prototype masonry. This is in agreement with the characteristics of prototype materials, shown in Table 2, which indicate that the values of diagonal tensile strength of AAC masonry do not vary significantly with increased compressive strength.

To obtain the characteristics of model masonry at seismic loading, 470/700/73 mm (length/height/thickness) model walls have been tested by subjecting them to cyclic in-plane lateral loading at constant precompression, i.e. at compressive stress/compressive strength ratio $\sigma_o/f_{c,M} = 0.20$, where σ_o = average compressive stress in the horizontal cross-section of the wall and $f_{c,M}$ = the compressive strength of model masonry. The precompression was higher than that in the walls of the tested models (see Table 6), but was applied since it represents the critical situtation with regard to deformability of walls in actual cases. Two types of model walls have been tested, namely 4 unreinforced walls and 6 walls, confined at the ends with vertical tie-columns in the same way as in the case of the model buildings. As can be seen in Fig. 5, unreinforced walls, tested as vertical cantilevers, failed in bending because of low compressive strength of AAC masonry. In the case of the confined walls, however, the flexural resistance of confined walls increased significantly despite the relatively small cross-sectional area of concrete and reinforcing steel of the tie-columns. Consequently, shear resistance was critical and the confined walls failed in shear (Fig. 6). In the case of the unreinforced walls, the virtual high ductility was the result of rocking of the upper part of the walls on the cracked section. Although the behaviour seems ductile and energy dissipation capacity high (see Fig. 5b), rocking caused heavy crushing of units and compression of the walls' upper part. In the case of confined walls, however, sudden resistance degradation took place once the shear cracks passed the concrete section of the tie-columns (see Fig. 6b). The resistance dropped to the level of that of the unreinforced walls. Since the tie-columns prevented rocking and caused shear failure, the displacement capacity was reduced with regards to the one observed during the tests of unreinforced walls.

Because of flexural failure, diagonal tensile strength, $f_{t,M}$, could not be evaluated from cyclic shear tests of unreinforced AAC masonry model walls. In the case of confined walls, however, equivalent value, which takes into consideration the contribution of tie-columns, attained $f_{t,eqv,M} = 0.15$ MPa. Since no information was available regarding the prototype value obtained by cyclic shear testing, the tensile strength obtained by diagonal compression

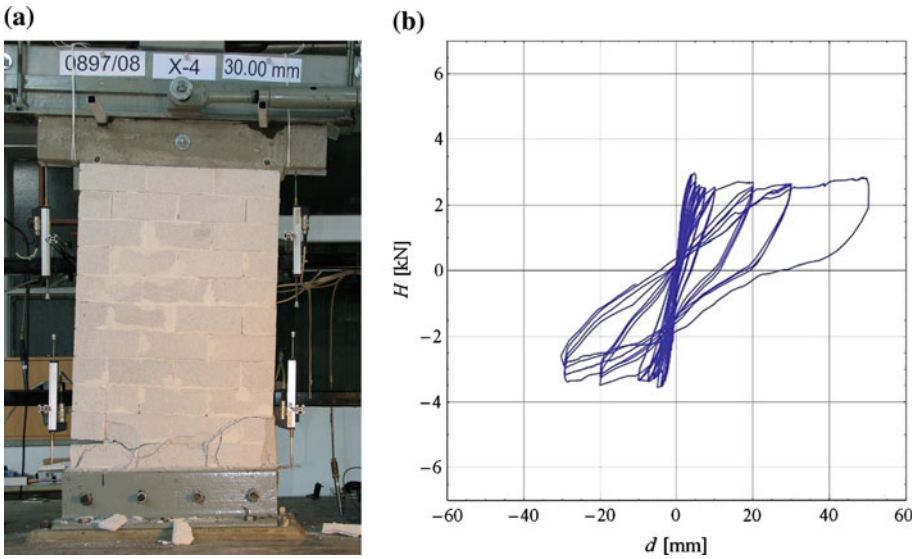

Fig. 5 Flexural failure mode of an unreinforced model masonry wall: **a** failure mechanism and lateral load—lateral displacement hysteretic loops (**b**)

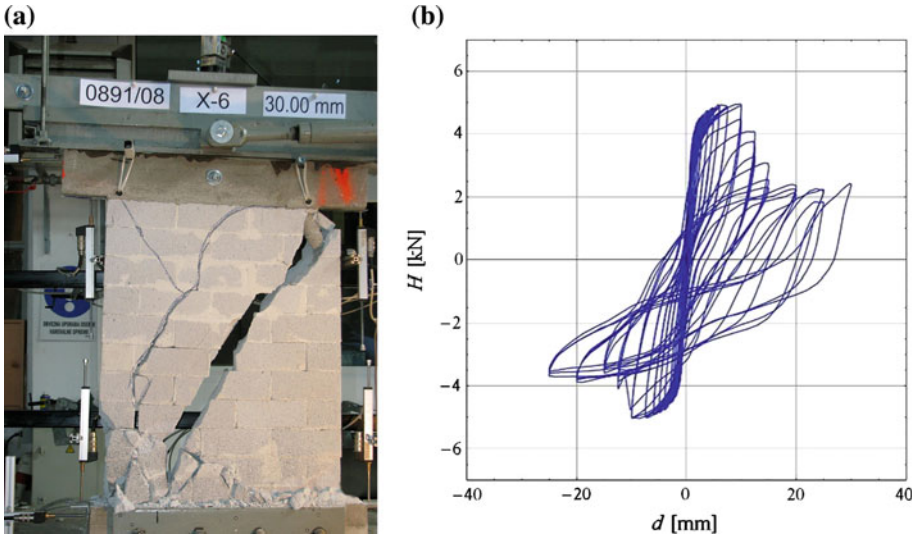

Fig. 6 Shear failure mode of a confined model masonry wall: **a** failure mechanism and lateral load—lateral displacement hysteretic loops (**b**)

tests was taken into consideration as the reference. Unexpectedly low value of equivalent shear deformability modulus, $G_{\mathrm{eqv,M}} = 90\,\mathrm{MPa}$, has been evaluated on the basis of the cyclic shear tests.

The values of elastic modulus, E_{M}, have been determined by compression tests. Average value obtained by testing 2 unreinforced model walls at compression was $E_{\mathrm{M}} = 4,360\,\mathrm{MPa}$.

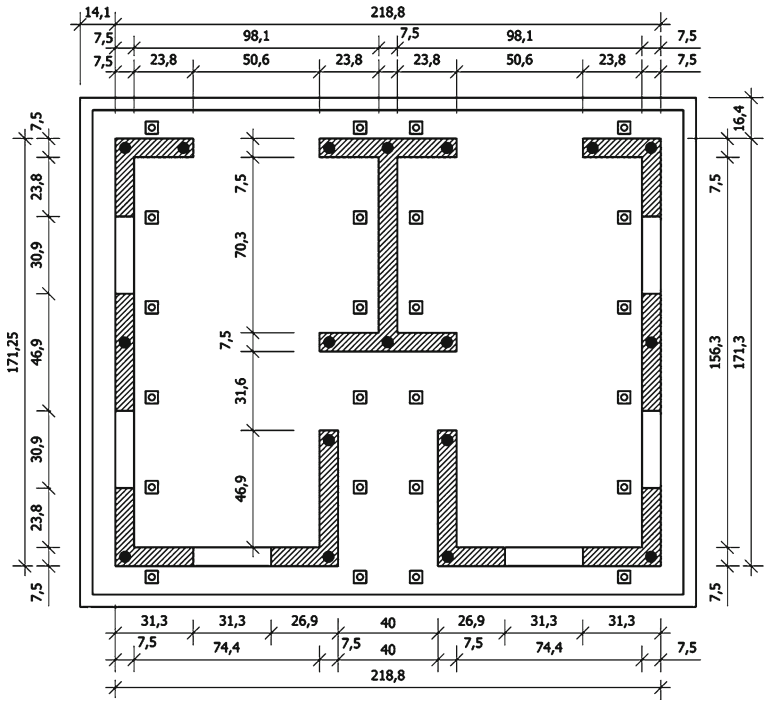

Fig. 7 Distribution of walls and dimensions of models in plan (in cm). The dimensions of foundation slab and position of holes to bolt the slab on the shaking table are also indicated

Micro-concrete with reduced strength was used for casting the slabs and concreting the tie-columns. Micro-concrete for tie-columns consisted of Portland cement, aggregate 0–2 mm, stone flour and water, whereas plasticizer was added when concreting the floor slabs. The compressive strength of concrete varied from 7.8 to 10.4 MPa in the case of the tie-columns and from 16.6 to 27.4 MPa in the case of the floor slabs. Same paste as in the case of the prototypes was used for the construction of the models' walls.

Steel with prototype characteristics was used for reinforcing the floor slabs, vertical tie-columns and horizontal bond beams. To scale the tension capacity of reinforcing steel, the area of the cross-section of reinforcement was reduced in accordance with the force scale factor, $S_F = 16$. Fully annealed wire of appropriate diameter, available on the market, was used. However, since the material properties are not standardized, the yield stress of model reinforcing steel depended on the diameter. In the case Ø 3.5 mm diameter bars the yield stress was 210 MPa, in the case of Ø 3.8 mm bars 480 MPa, and in the case of Ø 4.2 mm bars 220 MPa.

3.3 Construction of models

As can be seen in Fig. 7, the dimensions of all models in plan were 1.71 × 2.19 m, and clear storey height was equal to 0.675 m. By considering the thickness of floors, the height of three-storey model M1 was 2.03 m, the heigth of model M2 was 1.99 m, and the height of four-storey model M3 was 2.65 m. For practical reasons, the thickness of peripheral and internal wall was the same (7.5 cm) in all cases. Typical vertical sections and schemes of

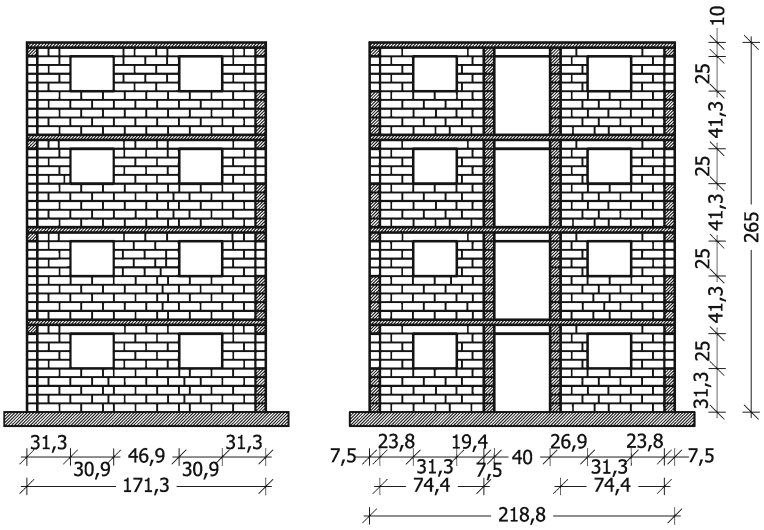

Fig. 8 Vertical sections and scheme of laying the AAC blocks in the case of model M3 (in cm)

Fig. 9 Building the models

laying the blocks in the case of model M3 are shown in Fig. 8. Laying the blocks during the construction of the models is shown in Fig. 9.

Floor structures of model M1 represented prefabricated Ytong® floors, consisting of inversely placed r.c. T-shape beams, which support AAC filler blocks and are connected with rectangular r.c. transverse beams, placed at regular intervals. Prefabricated elements are not covered with r.c. topping, as required by the code, but with only 1–2 mm thick layer of thin layer mortar, same as the mortar used for laying the AAC blocks. To simplify the construction of model M1, T-shaped beams have been cast in place, but the procedure of laying the filler blocks and topping the slab was the same as in the case of the prototype (Fig. 10). In the case of prefabricated Ytong® floors, horizontal bond beams are cast in two different ways. Above the last course of internal walls, the reinforcement of bond beams is placed in U-shaped AAC

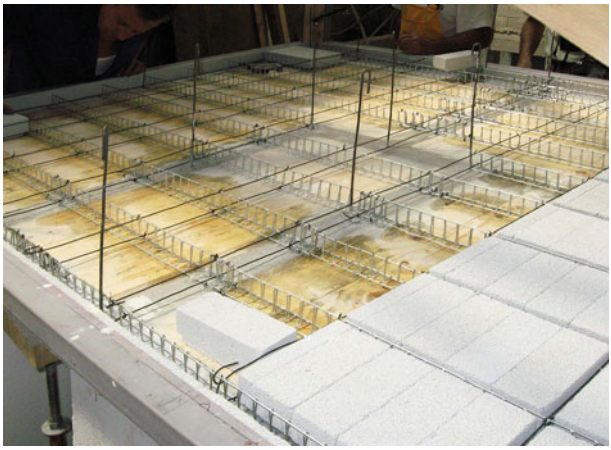

Fig. 10 Reinforcement of T-beams and AAC filler blocks of Ytong® floors before concreting. Reinforcement of tie-columns can be also seen

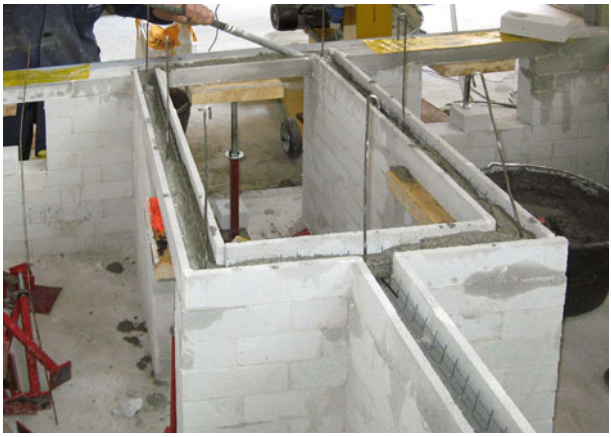

Fig. 11 Concreting the bond-beams above internal walls. Reinforcement of bond-beams and tie-columns can be also seen

elements. Above the peripheral walls, however, the reinforcement is placed along the walls between the floor filler blocks and outer edge of the walls (Fig. 11).

One Ø 4.2 mm reinforcing bar with yield stress 220 MPa or one Ø 3.8 mm reinforcing bar with yield stress 480 MPa has been placed in the vertical tie-columns in the case of models M1 and M2, or M3, respectively. Horizontal bond beams have been reinforced with one Ø 3.5 mm diameter bar (yield stress 210 MPa).

Floor structures of models M2 and M3 are monolithic r.c. two-way slabs (Fig. 12). They are reinforced at the bottom and top with reinforcing mesh; U-shaped stirrups are placed along the perimeter. The models have been built on r.c. foundation slabs, which had built-in steel elements for transportation and holes to bolt the slab with the model on it on the steel platform of the shaking table after the transport.

Before testing, steel blocks have been fixed to the floors to simulate the weight of the prototype floor topping (1.50kN/m^2) and part of the live load ($p = 2.00$kN/m^2), which

Fig. 12 Reinforcement of monolithic r.c. slabs

Fig. 13 Weights, fixed on the top floor slab of model M3

has to be considered in the design of buildings in seismic situation ($\psi_{E,i}p = \varphi\psi_2 p = 0.5 * 0.3 * 2.00 = 0.30\text{kN/m}^2$) according to Eurocode (CEN 2004). The weight of the prototype roof was 1.25kN/m^2. Amount of mass added to the floors by strictly respecting the modelling rules was not sufficient to induce inertia forces large enough to cause damage to models, even when subjected to highest available intensity of motion of the shaking table. To solve the problem and increase the inertia forces at the same intensity of seismic excitation, additional weights have been fixed on the floors. This, however, distorted mass distribution and, hence, dynamic similitude, but did not affect the similitude of failure mechanisms (see Table 6). When referring the results of model tests to prototype buildings, the modification of similitude relationships was taken into consideration.

Instead of 210, 560 kg mass (680 kg on the top floor) weights have been fixed to the floor slabs of all models. The weights (steel blocks), fixed on the top floor slab of model M3, are shown in Fig. 13. As an example, the distribution of masses, concentrated at floor levels in the case of model M3, is given in Table 5.

By taking into consideration the design seismic situation in the case of the prototype and the actual situation in the case of the models with additional masses, the average working

Table 5 Masses of model M3, concentrated at floor levels (in kg)

	1st storey	2nd storey	3rd storey	4th storey
Walls	175	175	175	79
Floor	406	406	406	406
Weights	560	560	560	680
Total	1,141	1,141	1,141	1,165
Grand total	4,588 kg			

Table 6 Comparison of precompression ratio in the walls of prototype and models (average compressive stress/compressive strength of masonry ratio)

Model	σ_{oP} (MPa)	$\sigma_{oP}/f_{c,P}$	σ_{oM} (MPa)	$\sigma_{oM}/f_{c,M}$
M1	0.093	0.030	0.044	0.030
M2	0.131	0.042	0.055	0.037
M3	0.174	0.076	0.073	0.049

$f_{c,P} = 3.14$ MPa (strength class 4), $f_{c,M} = 1.49$ MPa

stress/compressive strength of masonry ratios have been assessed and compared to those in the case of the prototypes. The calculated values are compared in Table 6. Although the amount of the mass, fixed to the floor, was more than double of that needed, the correlation between the stress state in models' walls and model materials' compressive strength remained quite similar to the situation in the prototype buildings. By comparing the prototype and model values, it can be concluded that additional weights did not affect the failure mechanism.

In Table 6, σ_{oP} and σ_{oM} are the average compressive (working) stresses in the walls of the prototype and model, respectively, and $f_{c,P}$ and $f_{c,M}$ are the compressive strengths of prototype and model masonry, respectively.

3.4 Seismic loading and testing procedure

Shaking table at ZAG is a simple device, consisting of a rigid foundation steel box, fixed to the r.c. laboratory testing floor, and a moveable, 2.0/3.2 m steel platform, onto which the foundation slab with the model is bolted and which is moved by means of a programmable hydraulic actuator. Teflon bearings on the foundation box provide for a controlled, quasi frictionless uni-directional motion of the shaking table, without uplifting or lateral motion (Fig. 14). Hydraulic actuator, fixed on the steel reaction wall, is displacement controlled. Schenck PL 160N actuator (force capacity ± 160 kN, displacement capacity ± 125 mm) coupled with hydraulic pump. The capacity of the pump (245 l min^{-1} at 280 bar) is enough to accurately drive the payload of up to 5,000 kg mass with motion of typical earthquake spectral characteristics, needed when testing models of up to 1:5 scale (Fig. 15). The calibration measurements have shown that the moveable platform is rigid enough for carrying the bending loads, developed as a result of interaction between the model and platform during the shaking tests.

N-S component of Petrovac record of Montenegro earthquake of April 15, 1979, has been used to simulate the earthquake ground motion (Fig. 16). The duration of the record is 48 s (strong phase is 24 s long), with peak ground acceleration 0.43 g. The acceleration record has been scaled assuming that true models will be tested. Consequently, the duration has

Fig. 14 Simple shaking table at ZAG with model M1 ready for testing

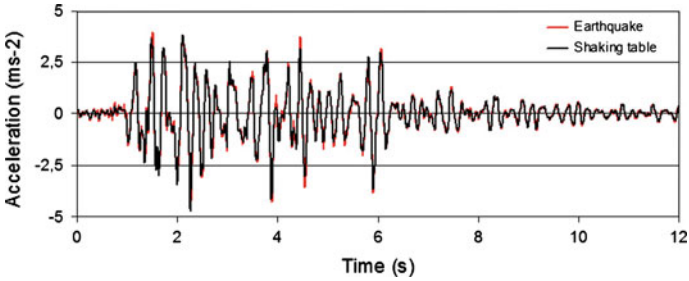

Fig. 15 Correlation between input acceleration time history, used to drive the actuator, and actual accelerations, measured on the shaking table (true model, 1:4 scale, 3,000 kg payload)

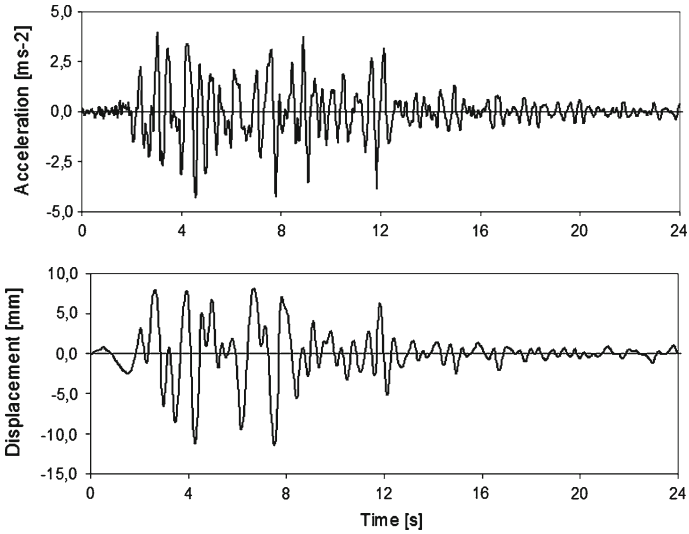

Fig. 16 Strong phase of the N-S component of Petrovac record of Montenegro earthquake of 1979

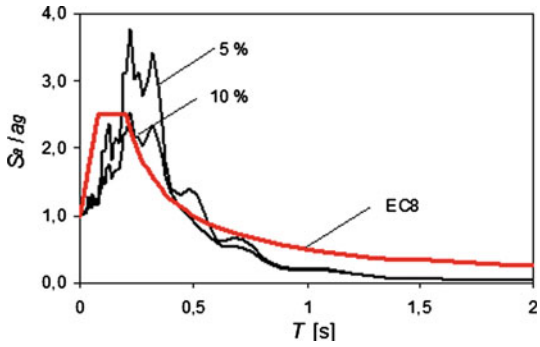

Fig. 17 Normalised response spectra of the modelled ground motion accelerogram compared with the scaled Eurocode 8 elastic response spectrum

Fig. 18 Instrumentation and position of model M1 on the shaking table

been reduced by time scale factor $S_t = S_L^{1/2} = 2$ to 12 s, whereas the accelerations remained unchanged. As can be seen in Fig. 17, the response spectrum of the model earthquake for 10% of critical damping is in relatively good agreement with the Eurocode 8 elastic spectrum for 5% of critical damping, scaled at the same time scale. It can be also seen that by adding masses to floors, the first natural frequency of vibration of models moved towards the flat part of the spectrum. In the case of Model 1, for example, which has been also tested with design mass fixed to the flooors, the frequency shifted from 21 Hz (first natural period T = 0.048 s) to 14.1 Hz (T = 0.071 s).

All models have been instrumented with a set of displacement transducers and accelerometers, located at both corners and in the middle of the slabs at each floor level. Whereas the accelerometers were fixed to the floor slabs, the displacements transducers were fixed to an external steel frame so that the absolute displacements of the models, i.e. displacements relative to the testing floor have been measured. To evaluate the inter-storey drift at the ground floor and assess the intensity of shaking, the displacements and accelerations of the shaking table have been also measured. The position of the models M1 and M3 on the shaking table and instrumentation is shown in Figs. 18 and 19, respectively.

All models have been tested by subjecting them to the same sequence of test runs. The intensity of excitation was gradually increased until the ultimate limit state of collapse was

Fig. 19 Instrumentation and position of model M3 on the shaking table

attained. The designation of test runs represents target shaking table acceleration, expressed in percent of the maximum acceleration of the model earthquake. Test run R100 represented excitation with the model earthquake (100%; $a_{max} = 0.43\,g$), whereas test runs R25 and R200, for example, represented excitations with 25% and 200% of intensity of the model earthquake, respectively. Models M2 and M3 were subjected to seismic excitation along the axis of symmetry. Since the direction was considered critical for prefabricated floors, Model M1, however, was tested with seismic excitation orthogonal to the axys of symmetry.

The response was recorded with two video cameras. After each test run, the models have been inspected for damage and first natural frequency of vibration was neasured by exciting free vibrations of the model by hitting the top floor slab with impact hammer.

4 Test results

4.1 Failure mechanisms

Typical shear mode of vibration with prevailing shear failure of walls in the direction of excitation has been observed. Although some cracks occurred also in the upper storeys, the amount of damage was less severe, so that, eventually, all models collapsed because of the failure of the walls in the ground storey (Figs. 20 and 21). Consequently, storey mechanism where the relationship between the base shear and first storey (interstorey) drift defines the resistance of the structure, determined the failure mechanism. The first mode of vibration was predominant and the torsional oscillations were negligible despite the asymmetry along the longer axis of the models. The effect of tie-columns was paramount: they have maintained the integrity of the walls despite their heavy damage after the attainment of maximum resistance. However, no influence of the amount of reinforcing steel and tie-columns diameter on the amount of damage and resistance of the model has been observed. Typical damage at

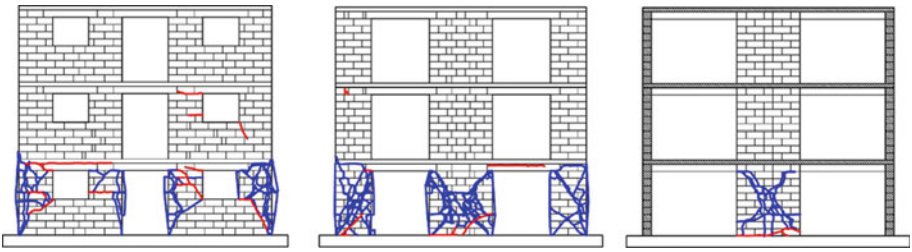

Fig. 20 Propagation of damage to the in-plane loaded walls of model M2 at damage limit (*red*) and ultimate state (*blue*). Storey failure mechanism is clearly visible

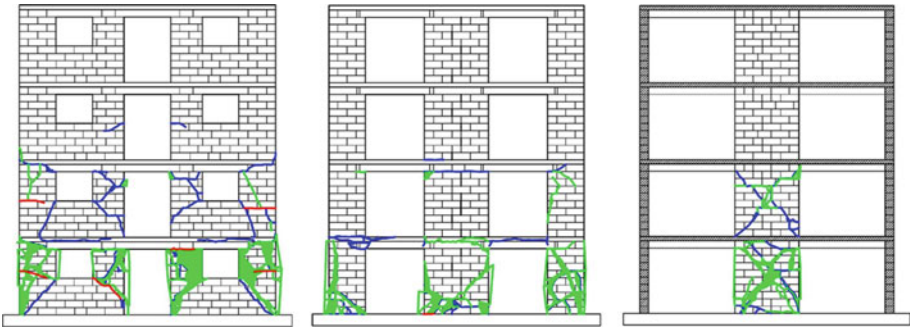

Fig. 21 Propagation of damage to the in-plane loaded walls of model M3 at damage limit (*red*), maximum resistance (*green*) and ultimate state (*blue*). Storey failure mechanism is clearly visible

Fig. 22 Damage to the walls in the ground floor of model M2 at ultimate state

ultimate state is shown in Figs. 22 and 23. No damage to prefabricated Ytong® or reinforced concrete slabs has been observed.

4.2 Dynamic response and seismic resistance

The analysis of vibrations indicated that all models vibrated as shear systems with prevailing first natural mode of vibration. The contribution of higher modes, including torsional, was

Fig. 23 Damage to the walls in the ground floor of model M3 at ultimate state

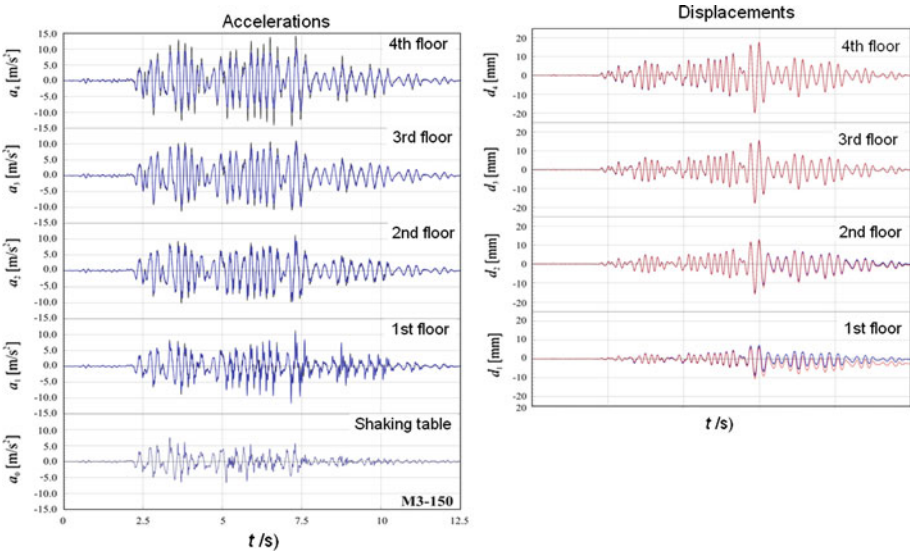

Fig. 24 Acceleration and displacement response time history of model M3 at maximum resistance

minimal. As an example, the acceleration and displacement response time history, recorded during the testing of model M3 at the attained maximum resistance (test run R200), is shown in Fig. 24.

After each test run, the first natural frequency of vibration has been determined by exciting free vibration of the model by hitting the top floor slab with an impact hammer. The first natural frequency decay with increased damage to the walls can be seen in Table 7.

As can be seen, practically no difference in initial frequency of vibration has been measured in the case of models M1 and M2, although the direction of excitation was different. Whereas model M1 vibrated along the strong axis, i.e. axis of symmetry (wall/floor ratio 8.3%), model M2 vibrated along the weak axis (wall/floor ratio 5.8%). Since model M3 was one storey higher than models M1 and M2, lower initial frequency of vibration was not

Table 7 First natural frequency of vibration decay

After test run	Natural frequency (s^{-1})		
	Model M1	Model M2	Model M3
R005	–	14.5	10.9
R025	14.1	14.1	10.1
R050	13.1	13.7	9.9
R100	10.6	13.7	9.8
R150	9.9	–	6.8
R200	9.9	11.1	–

against expectations. In all cases, a decay in the first natural frequency has been observed after each test run, even in the case where no visible damage to the walls has been observed.

On the basis of the measured acceleration time histories and known masses of the models, concentrated at floor levels, horizontal inertia forces (shear forces) induced in the models during testing at individual floor levels can be estimated by simply multiplying the measured accelerations and masses:

$$S_{\mathrm{i}} = \sum_{\mathrm{i}}^{\mathrm{n}} m_{\mathrm{i}} a_{\mathrm{i}}, \tag{2}$$

where:
S_{i} shear force acting at the i-th floor level,
m_{i} mass, concentrated at i-th floor level (see Table 5),
a_{i} acceleration, measured at i-th floor level,
n number of floors.

Maximum base shear, induced during testing, represents the resistance of the models to seismic loads. It is determined as the maximum of the sum of inertia forces, induced at individual floors of the models at the same instant of time:

$$BS_{\max} = \max\left(\sum_{1}^{\mathrm{n}} m_{\mathrm{i}} a_{\mathrm{i}}\right). \tag{3}$$

The values of maximum measured base shear are given in Table 8. For comparison, maximum measured shaking table accelerations, $a_{\mathrm{o,max}}$, are also given in the table. As can be seen, maximum base shear, induced in the models during shaking tests, which represents the resistance of the models to seismic loads, did not depend significantly on the direction of excitation and number of stories. Theoretically, the resistance of model M1 (wall/floor ratio in the direction of excitation 8.3%) should be greater than the resistance of model M2 (wall/floor ratio 5.8%). Also, the resistance of model M3 with higher compressive stresses in the walls should be greater than resistance of model M2, tested in the same direction. However, although shear failure mode of walls in the direction of excitation determined the mechanism, the contribution of orthogonal walls to box-type behaviour of the models was also important.

In Table 8, the values of the base shear are given also in the non-dimensional form of the base shear coefficient, i.e. the ratio between the maximum base shear, $BS_{\max}$, and the weight of the model, W : $BSC_{\max} = BS_{\max}/W$. At the same actual resistance of the critical storey, the base shear coefficient values decrease with the increased weight of the models.

Table 8 Maximum base shear and base shear coefficient

Model	$a_{o,max}$ (g)	BS_{max} (kN)	W (kN)	BSC_{max}
M1	1.37	45.02	27.46	1.64
M2	1.28	45.94	33.82	1.36
M3	0.77	41.89	45.01	0.93

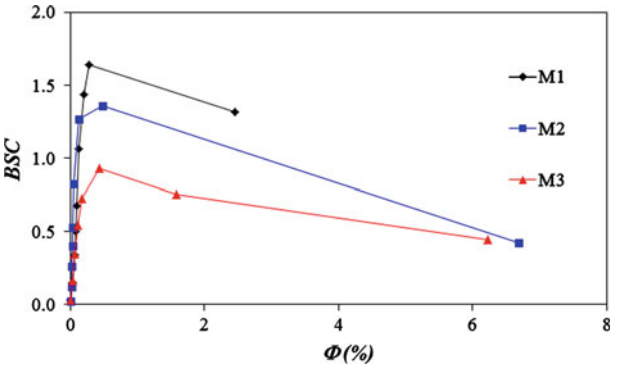

Fig. 25 Resistance curves. Base shear coefficient—interstorey drift angle relationships obtained by testing

Resistance curves have been evaluated as the envelopes representing relationship between the peak values of the base shear and corresponding interstorey drift angle, evaluated during each successive test run. Storey drift angle is defind as the ratio between the relative storey displacement, d, and storey height, h : $\Phi = d/h$ (in %) The resistance curves are shown in Fig. 25. Substantial ductility capacity can be seen as a result of tie-columns, which provided the integrity of structural system deep into the non-linear range of vibration. Although rupture of reinforcing steel of several tie-columns in tension has been observed in the case of models M1 and M2, this had no visible effect on the seismic behaviour.

Three characteristic limit states have been defined on resistance curves:

- Damage (crack) limit state, defined by the maximum base shear and interstorey drift during test run where the first visible damage to structural walls has been observed, causing significant stiffness degradation;
- Maximum resistance, defined by the interstorey drift where the maximum base shear, representing the resistance of the model, has been evaluated;
- Ultimate limit state (collapse), defined by the maximum interstorey drift and corresponding base shear, measured during test run where the model partly or completely collapsed.

The evaluated values of the base shear coefficient and corresponding interstorey drift angle at characteristic limit states are given in Table 9.

As can be seen, the values of interstorey drift angle at damage (crack) limit and maximum resistance limit states are in good correlation with the values, reported in previous research (Alcocer et al. 2004; Tomaževič 2007; Tomaževič and Weiss 2010).

4.3 Energy dissipation capacity and structural behaviour factor

To obtain information regarding energy dissipation capacity, hysteretic behaviour of the tested models, i.e. the relationship between the storey shear and relative storey displacement

Table 9 Base shear coefficient, BSC, and interstorey drift angle, Φ, at characteristic limit states

Limit state	Model M1			Model M2			Model M3		
	Test run	BSC	Φ (%)	Test run	BSC	Φ (%)	Test run	BSC	Φ (%)
Damage (crack) limit	R200	1.54	0.23	R150	1.29	0.36	R100	0.83	0.30
Maximum resistance	R250	1.64	0.28	R250	1.36	0.49	R150	0.93	0.43
Collapse	R300	1.31	2.55	R250	0.42	6.69	R250	0.45	6.22

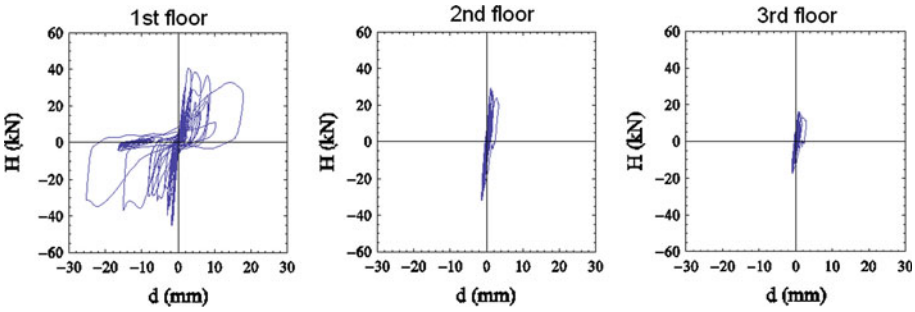

Fig. 26 Storey shear—interstorey drift hysteresis loops, measured during the testing of model M1 (test run R250)

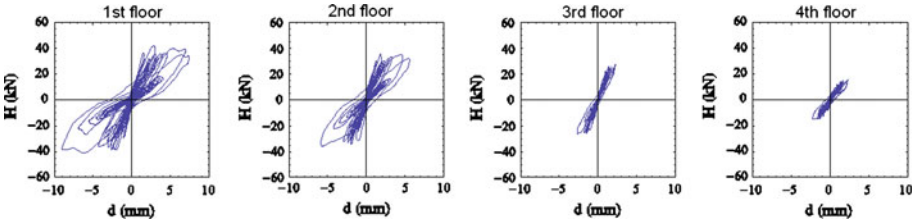

Fig. 27 Storey shear—interstorey drift hysteresis loops, measured during the testing of model M3 (test run R150)

(interstorey drift) has been also analysed. Typical hysteretic relationships between the storey shear and interstorey drift in the non-linear range of behaviour of models M2 and M3 are shown in Figs. 26 and 27.

Taking advantage of the measured response, the correlation between the input and dissipated energy of the tested models has been analysed. For each of the tested models, the input energy, induced to the system by means of hydraulic actuator, has been estimated by the following equation (after Bertero and Uang 1992):

$$E_{\text{inp}} = \int_0^t \left| \left(\sum_{\text{i}=1}^{\text{n}} m_{\text{i}} a_{\text{i}}(\tau) \right) \upsilon_{\text{i}}(\tau) \right| \text{d}\tau, \tag{4}$$

Table 10 Ratio between the dissipated hysteretic, E_{hys} and input energy, E_{inp}, in the case of testing of model M3

Test run	E_{hys}/E_{inp}				
	1st floor	2nd floor	3rd floor	4th floor	Total
R005	0.02	0.00	0.02	0.00	0.03
R025	0.00	0.00	0.01	0.00	0.01
R050	0.00	0.00	0.00	0.00	0.00
R075	0.00	0.00	0.00	0.00	0.00
R100	0.00	0.00	0.00	0.00	0.00
R150	0.19	0.10	0.02	0.02	0.31
R200	0.64	0.22	0.03	0.02	0.89
R250	0.64	0.09	0.01	0.01	0.75

where
E_{inp} input energy from the beginning to time t,
m_i mass, concentrated at i-th floor level,
$a_i(\tau)$ acceleration time history, measured at i-th floor level,
$v_i(\tau)$ velocity time history at i-th floor level,
n number of stories;
$d\tau$ time increment.

Dissipated hysteretic energy, E_{hys}, has been estimated on the basis of the measured storey shear—relative storey displacement hysteresis loops:

$$E_{hys} = \sum_{i=1}^{n} \int_{0}^{u_i(t)} H_i du_i, \tag{5}$$

where
E_{hys} the dissipated hysteretic energy from the beginning to time t,
H_i storey shear, measured at i-th floor level,
u_i relative storey displacement, measured at i-th floor level,
du_i increment of relative storey displacement, measured at i-th floor level.

As the analysis indicated, in the initial phases of testing, where the linear behaviour of the models has been observed, energy has been dissipated by viscous damping. Only when significant damage had already occurred to the walls, a significant part of the input energy, up to 75% in the ground floor at ultimate state, has been dissipated by hysteretic behaviour. The dissipated hysteretic/input energy ratio along the height of the models also indicates the predominant storey mechanism. In all cases, the dissipated hysteretic/input energy ratio was much higher in the ground floor than in the upper stories. The dissipated hysteretic/input energy ratio in the upper storeys was very low even at the ultimate state of collapse. As typical example, the correlation between the dissipated hysteretic and input energy for the case of testing of model M3 is presented in Table 10.

If a regular structure possesses displacement and energy dissipation capacity, it may be designed for ultimate design loads using conventional elastic analysis models. Ultimate design loads are equal to elastic seismic forces, which would develop in an equivalent ideal elastic structure, reduced by a factor, called force reduction factor or structural behaviour factor, q. According to Eurocode 8 (CEN 2004) and based on the assumption of equality

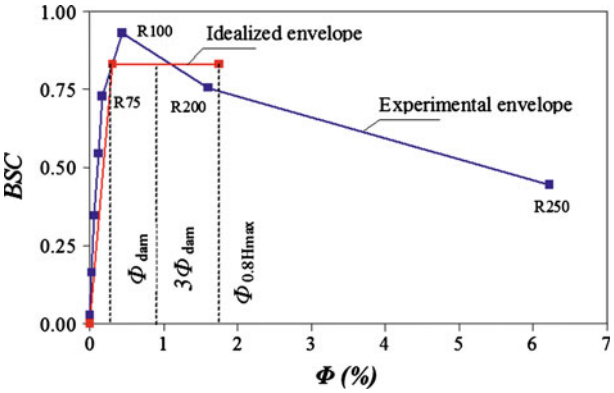

Fig. 28 Evaluation of structural behaviour factor q for the case of model M3

of displacements of elastic and nonelastic response of the same structure to the same earthquake, "the behaviour factor q is an approximation of the ratio of the seismic forces that the structure would experience if its response was completely elastic with 5% viscous damping to the minimum seismic forces that may be used in the design—with a conventional elastic analysis model—still ensuring a satisfactory response of the structure". Taking into consideration the assumption of equality of energies, however, the structural behaviour factor, q, can be also expressed in terms of the global ductility factor of the structure under consideration, $\mu_u = d_u/d_e(\Phi_u/\Phi_e)$, where $d_e(\Phi_e)$ = the displacement (drift) of the structure at the elastic limit and $d_u(\Phi_u)$ = the displacement (drift) at ultimate limit.

The latter assumption has been used to evaluate the available ductility and force reduction factor in the case of the tested models. Consequently, experimentally obtained resistance curves have been idealized as bi-linear, elastic—ideal plastic relationships (Fig. 28). Elastic limit has been defined by the displacement (drift) at the initiation of damage (cracks) $\Phi_e = \Phi_{cr}(\Phi_{dam})$ and called damage (crack) limit. Since q-factors are used for the design, ultimate limit is defined by taking into consideration damage limitation criterion. On the basis of correlation between damage to masonry walls and displacement capacity (Tomaževič 2007), it has been found that the smaller value of displacement (drift) where the resistance degrades to 80% of the maximum, as proposed by (CEN 2004), and displacement (drift) at 3-times the value of the displacement (drift) at the damage (crack) limit, $\Phi_{d,u} = \min\{\Phi_{0,8Rmax}; 3\Phi_{dam}\}$, can be defined as the ultimate design limit.

The results of such evaluation are given in Table 11. Although damage limitation criterion ($\Phi_{d,u} = 3\Phi_{dam}$) has been found critical in all cases, the values of factor q have been evaluated also on the basis of strength degradation criterion ($\Phi_{d,u} = \Phi_{0.8Hmax}$). As the comparison shows, the values of factor q, evaluated on the basis of damage limitation criterion are well within the range of values, proposed by Eurocode 8 for confined masonry structures (2.0–3.0). In the case of strength degradation criterion, however, the values are much higher.

It should be mentioned that the values of behavior factors q, given in Table 11, have been evaluated by taking into consideration the actual, and not the design resistance capacity of the tested models. In practical verification procedures, however, mechanical characteristics of materials are reduced with partial safety factors. Besides, conventional elastic analysis methods do not consider redistribution of seismic forces. As a result, the calculated values of design resistance usually underestimate the actual resistance capacity of the structure. As has been already shown (Magenes 2006), mean values of overstrength factors for masonry

Table 11 Structural behaviour factor, q, evaluated on the basis of displacement capacity of the tested models

Model	M1	M2	M3
Φ_{dam} (%)	0.23	0.36	0.30
$\Phi_{d,u} = 3\Phi_{dam}$ (%)	0.71	1.08	0.90
$\mu_{d,u} = \Phi_{d,u}/\Phi_{cr}$	3.00	3.00	3.00
$q = (2\mu_{d,u} - 1)^{1/2}$	2.24	2.24	2.24
$\Phi_{d,u} = \Phi_{0.8Hmax}$ (%)	2.46	2.27	2.33
$\mu_{d,u}{}^{a} = \Phi_{0.8Hmax}/\Phi_{cr}$	10.69[a]	6.31[a]	7.77[a]
$q^{a} = (2\mu_{d,u}{}^{a} - 1)^{1/2}$	4.52[a]	3.41[a]	3.81[a]

[a] Values have been obtained by considering strength degradation criterion

structures in the case of traditional verification methods may vary from 1.8 to 2.4, depending on masonry construction system.

4.4 Prototype values

When referring test results to prototype buildings, the values measured on the models should be conversed by taking into account the influence of inaccurate modelling of material properties as well as the influence of masses, added to floors in order to induce large enough inertia forces during seismic excitation. As has been shown, the mechanical properties of AAC masonry were modelled relatively well. Compressive strength was reduced almost at geometry scale, as required by the laws of complete similitude, but the diagonal tensile strength remained the same. Like in the case of prototype AAC masonry, where diagonal tensile strength is almost constant at all three strength classes. Consequently, only minor reduction would have been necessary.

However, additional experimental evidence is needed to explain and confirm the unusual relationship between the compressive and tensile strength of AAC masonry. As has been shown, shear failure mechanism governed the behaviour of the tested models. Therefore, test results were evaluated assuming that the strength of model materials was the same as the strength of the prototype materials. Consequently, when converting test results to prototype, the measured accelerations have been reduced by acceleration scale factor $S_a = 4$ (shear resistance of model masonry walls was 4-times greater than assumed by the laws of true modelling).

Then, as a result of additional masses, the inertia forces developed in the models were greater than forces developed if theoretically required, design masses were fixed to floor slabs. Consequently, the measured values of accelerations have been multiplied by mass correction factor $S_{a,corr} = m_{tot,a}/m_{tot,d}$, a factor taking into consideration the ratio between the actual total mass (weight), $m_{tot,a}$, and design total mass (weight) of the models, $m_{tot,d}$. Actual and design total masses of models with calculated mass correction factors are given in Table 12.

The resulting prototype values of the base shear coefficient and interstorey drift at characteristic limit states are given in Table 13.

As can be seen, all buildings of the tested type and size will exhibit adequate seismic behaviour, if constructed as confined masonry system. Shaking table tests confirmed the important role of vertical tie-columns, which improved the resistance capacity of the walls, prevented disintegration at ultimate state and ensured integrity of the structure up to collapse. As has been observed by testing plain and confined AAC masonry model walls, tie-columns

Table 12 Actual and design total masses of models and calculated mass correction factors

Model	M1	M2	M3
Actual total mass (kg)	2,799	3,447	4,588
Design total mass (kg)	1,638	2,286	3,040
Mass correction factor ($S_{a,corr}$)	1.71	1.51	1.51

Table 13 Prototype values of base shear coefficient, BSC, and interstorey drift, Φ, at characteristic limit states

Limit state	M1		M2		M3		Demand[a]
	BSC	Φ (%)	BSC	Φ (%)	BSC	Φ (%)	BSC_d
Damage limit	0.67	0.23	0.48	0.36	0.32	0.30	–
Maximum resistance	0.70	0.28	0.51	0.49	0.35	0.43	0.30
Collapse	0.56	2.55	0.17	6.69	0.17	6.22	–

[a] Demand: design ground acceleration $BSC_d = a_g = 0.30$, where $S = 1.24$—soil factor and $a_g = 0.25$—design ground acceleration for type A ground (CEN 2004)

Table 14 Correlation between the experimental and calculated resistance of tested model AAC masonry walls

Dimensions l/h/t (mm)	Description	Mechanism	$H^a_{max,exp}$ (kN)	H_{fl}(kN)	$H_{fl,conf}$(kN)	H_s(kN)
470/700/73	Unreinforced	Flexural	3.19	2.62	–	5.93
470/700/73	Unreinforced	Flexural	3.15	2.62	–	5.93
470/700/73	Unreinforced	Flexural	3.26	2.62	–	5.93
470/700/73	Unreinforced	Flexural	3.34	2.62	–	5.93
470/700/73	Tie-columns as M1	Shear	5.18	2.62	4.90	5.93
470/700/73	Tie-columns as M1	Shear	5.00	2.62	4.90	5.93
470/580/74	Tie-columns as M3	Shear	5.79	3.21	7.27	6.01
470/580/72	Tie-columns as M3	Shear	6.47	3.12	7.27	5.85
470/580/72	Tie-columns as M3	Shear	6.61	3.12	7.27	5.85
470/580/72	Tie-columns as M3	Shear	6.32	3.12	7.27	5.85

[a] $H_{max,exp}$—experimentally obtained maximum lateral resistance

significantly improved the resistance capacity, although the dimensions of tie-columns did not completely comply with code requirements. As a result of low compressive strength and relatively high tensile strength of AAC masonry, flexural resistance was critical in the case of unreinforced AAC walls. Confined walls, however, where the tie-columns improved the flexural capacity, failed in shear. As can be seen in Table 14, shear resistance of confined model walls was significantly higher than flexural resistance.

5 Modelling

Using advantage of the observed storey shear mechanism, a simple model has been proposed to simulate the seismic response of tested buildings, idealised as lumped mass systems. Storey resistance curves, representing the skeleton curve of hysteretic behaviour, is calculated by using a push over method, originally developed in 1976 (Tomaževič 1978). Hysteretic

behaviour is simulated by simple rules, defined by experimentally determined damage and energy dissipation based stiffness and strength degradation parameters.

5.1 Resistance curve

To investigate the influence of tie-columns on the seismic behaviour of AAC masonry walls, 4 unreinforced walls and 6 walls, confined at vertical borders with tie columns as in the case of models M1 (2 walls) and M3 (4 walls), have been tested by subjecting them to cyclic lateral in-plane loads at constant preloading, equal to 20% of the compressive strength of masonry. As shown in Figs. 5 and 6, unreinforced AAC masonry model walls failed in bending, whereas the walls, confined at vertical borders with tie columns, failed in shear. To explain these observations, the resistance of the tested walls was verified by using well known equations for calculation of the flexural resistance of unreinforced masonry:

$$M_{\mathrm{u}} = \frac{\sigma_{\mathrm{o}} \ tl^2}{2}\left(1 - \frac{\sigma_{\mathrm{o}}}{0,85 f_{\mathrm{c}}}\right), \tag{6}$$

and confined masonry wall sections (Tomaževič 1999):

$$M_{\mathrm{u,conf}} = F_{\mathrm{m,eqv}}\left(\frac{l-a}{2}\right) + A_{\mathrm{v}} f_{\mathrm{y}} z. \tag{7}$$

Flexural resistance is obtained by dividing the sectional resistance by height of the wall, taking into account boundary conditions:

$$H_{\mathrm{fl,conf}} = M_{\mathrm{u,conf}}/\alpha h. \tag{8}$$

Shear resistance of unreinforced masonry walls was calculated by Turnšek and Čačovič (1971):

$$H_{\mathrm{s}} = A_{\mathrm{w}} \frac{f_{\mathrm{t}}}{b}\sqrt{\frac{\sigma_{\mathrm{o}}}{f_{\mathrm{t}}} + 1}, \tag{9}$$

where:

H_{fl}, $H_{\mathrm{fl,conf}}$	flexural resistance of unreinforced and confined wall,
H_{s}	shear resistance of unreinforced wall,
$F_{\mathrm{m,eqv}}$	resultant of compressive stresses in equivalent compressive stress block, which takes into account concrete of the tie-columns;
σ_{o}	average compressive stress in the horizontal section of the wall due to preloading,
$f_{\mathrm{t}} = f_{\mathrm{ts,M}}$; $f_{\mathrm{c}} = f_{\mathrm{c,M}}$ (Table 4)	tensile and compressive strength of masonry,
f_{y}	yield stress of reinforcing steel,
l	length, h—height and t—thickness of wall,
a	length of the compressive stress block,
z	internal lever arm,
A_{v}	cross sectional area of longitudinal reinforcement of tie-columns,
A_{w}	wall area,
b	shear stress distribution factor, depending on the geometry of the wall and ratio between the axial and ultimate horizontal load. In the case of the wall with geometrical aspect ratio more than $h/l = 1.5$, b = 1.5,
α	coefficient, determining the position of moment inflection point.

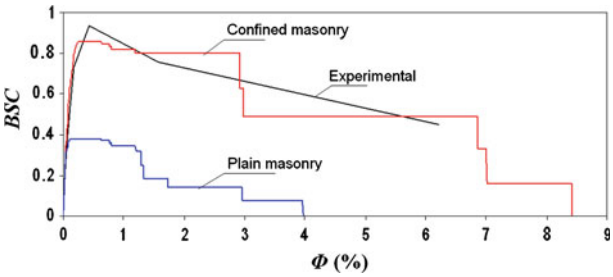

Fig. 29 Comparison of experimental and calculated resistance envelopes for the base floor of model M3

The results of calculation are given in Table 14. As can be seen, the influence of tie-columns on the failure mode and in-plane resistance of AAC masonry walls has been explained also by simple calculations. Moreover, the calculated results are in good correlation with experimental observations.

Since they assess the resistance of walls relatively well, Eqs. 6, 7, 8 and 9 have been used in the pushover analysis to determine the resistance of individual walls in the storey considered. In the actual procedure, each floor of building under consideration is modelled by springs, representing the walls, and rigid connectors, which connect springs to the mass-center of the floor. Each wall is modelled by two springs, one for the in-plane and one for out-of-plane resistance. Both springs are bilinear and are defined by three parameters: maximum resistance, $H_{\max}$, effective stiffness, K_e, and ultimate ductility factor, μ_u. While maximum resistance is determined as the lesser value of the flexural and shear resistances of a particular wall, given by Eqs. 6, 7, 8 and 9, stiffness is defined by:

$$K_e = \frac{G_M A_w}{1.2h\left(1 + 3.33\frac{G_M}{E_M}\left(\frac{h}{l}\right)^2\right)}, \tag{10}$$

where E_M and G_M are the modulus of elasticity and shear deformability modulus of model masonry, respectively. The results of calculation are shown in Fig. 29, where the experimental resistance curve, respresenting measured non-dimensional relationship between the base shear and storey drift for the case of model M3, is compared with the calculated curves. Two cases have been considered: the case of a fictitious unreinforced AAC masonry building and the actual case of the confined masonry structural system. As can be seen, taking into consideration the simplicity of calculations, good correlation between the experimental and calculated storey resistance curve has been obtained for the case of the confined masonry structure.

5.2 Dynamic response

To calculate the dynamic response, the building is idealised as a lumped mass system, with storey hysteresis rules defining the non-linear response. The hysteretic model is based on the idealisation of the calculated storey resistance curve with a tri-linear envelope, i.e. skeleton curve, determined by relative storey displacement and resistance at the damage limit state (crack limit, d_{cr}, H_{cr}), maximum resistance (d_{Hmax}, H_{max}) and ultimate limit state (d_u, H_{du}).

Hyteretic rules take account for the damage based stiffness, as well as energy based resistance degradation (Park et al. 1987; Tomaževič and Lutman 1996). In the direction of loading, the maximum previously attained displacement in the respective direction of loading

determines the stiffness. In unloading, a bilinear unloading path is assumed. Initial unloading stiffness, $K_{\text{unload,ini}}$, is a function of the maximum attained displacement, taking into account the stiffness degradation with increased structural damage:

$$K_{\text{unload,ini}} = K_{\text{e}} \left(1 + \left(\frac{K_{\text{u}}/K_{\text{e}} - 1}{d_{\text{u}}/d_{\text{cr}} - 1}\right)\left(\frac{d_{\max}}{d_{\text{cr}}} - 1\right)\right), \tag{11}$$

where K_{u} = the ultimate stiffness ($K_{\text{u}} = H_{\text{du}}/d_{\text{u}}$), and $d_{\max}$ = the maximum attained storey drift. Initial unloading aims at a point, defined as:

$$H_{\text{C}} = c_{\text{F}} H_{\text{R}}, \tag{12}$$

where c_{F} is a masonry type dependent parameter. With unloading stiffness defined and force at point C known, the drift at point C can be easily calculated. Passing point C, the unloading aims at the point of the maximum attained displacement in the respective direction of loading. Cylic shear tests of the particular type of walls are needed to evaluate the value of parameter c_{F}, by making equal the amount of dissipated energy during experiments and numerical simulation. Practically, the value of parameter c_{F} is determined by a try and error procedure, choosing the value which gives smallest difference between the calculated and experimentally obtained amount of dissipated energy. In the particular case studied, the resulting value was $c_{\text{F}} = 0.66$, with coefficient of variation 4.6%. Hysteresis rules are shown in Fig. 30.

Park et al. (1987) proposal is used to model the strength degradation. The proposal assumes that, once passing the maximum attained resistance H_{att}, the target displacement (drift) increases proportionally with the amount of dissipated hysteretic energy in one loading cycle, A_{hys}. The drift increment δd is calculated as:

$$\delta d = \beta \left(A_{\text{hys}}/H_{\text{att}}\right), \tag{13}$$

where, again, β is a parameter, which depends on the masonry type. Obviously, drift increments are calculated separately for positive and negative direction and the maximum attained force is stored separately for both directions.

Parameter β is also evaluated on the basis of results of cyclic shear tests. Displacement increments are assessed from the results of two consecutive phases with different displacement amplitudes, whereas β is evaluated for each cycle of loading. Obtained values are averaged to yield the final value for a specific type of masonry wall. In the particular case studied, the average value for all walls was 0.30 with coefficient of variation of 37.1%.

The dynamic analysis has been performed using Rayleigh viscous damping and Newmark time integration scheme with trapezoidal rule. Seismic forces acting on the model are obtained by multiplication of the mass matrix and measured accelerations of the shaking table. Time step in the analysis was 0.00625 s (about 1/16 of the initial first natural vibration period of model M3). Typical results of calculation are shown in Figs. 31 and 32. In Fig. 31, typical calculated hysteretic relationships between the base shear and first storey drift are compared with the relationships, measured during the response of model M3 in the non-linear range, after the attained maximum resistance during test run R200.

In Fig. 32, calculated and measured first story drift response time histories of model M3 are compared for the same test run. As can be seen, relatively good correlation has been obtained in both cases by using this, relatively simple numerical model.

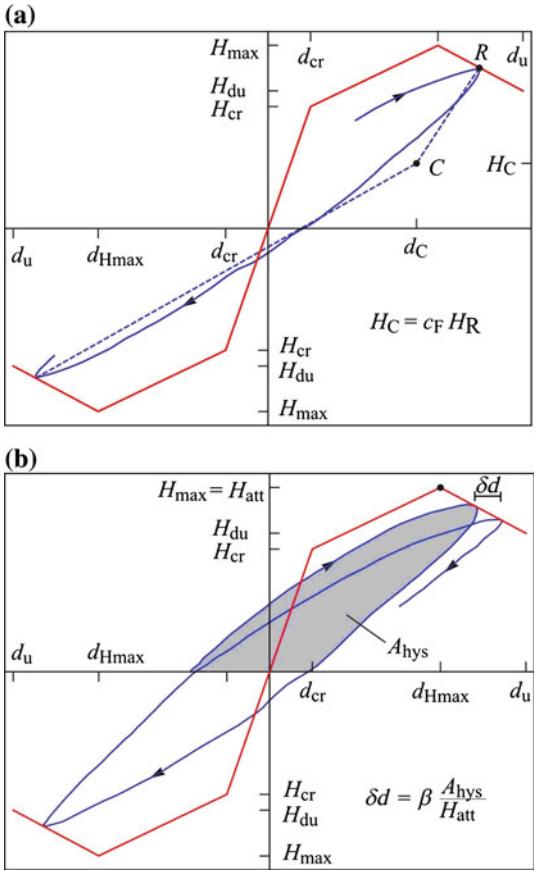

Fig. 30 Hysteretic rules. Unloading rules (**a**) and **b** strength degradation

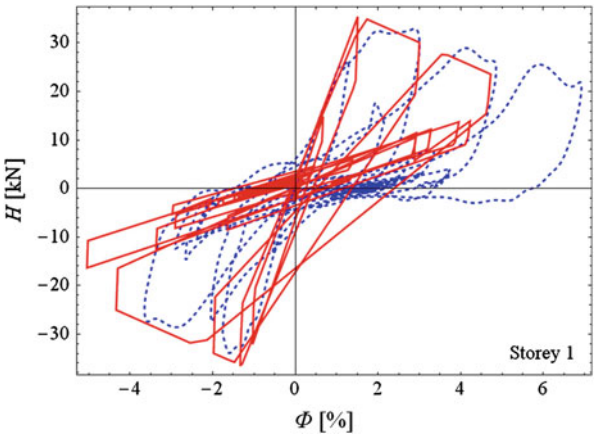

Fig. 31 Non-linear response of model M3 during test run R200. Base shear-first storey drift hysteretic relationships (*full line*—calculated, *dashed line*—experimental)

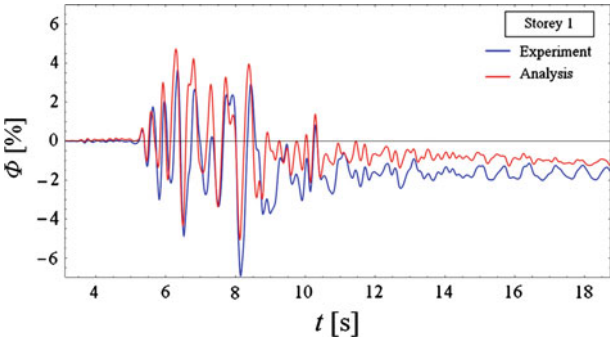

Fig. 32 First storey drift response time history of model M3 during test run R200

6 Conclusions

All buildings of the tested type will exhibit adequate seismic behaviour, if constructed as confined masonry system. The shaking table tests indicated the important role of vertical tie columns, which, in the particular situation of AAC masonry with high tensile/compressive strength ratio, significantly improved the resistance of the walls. Although the dimensions of the tie columns did not completely comply with code requirements, the tie columns prevented flexural failure of the walls and activated the available higher shear resistance capacity. At ultimate state, the tie columns prevented the disintegration of the walls and ensured the integrity of the structure up to collapse.

The resistance of all buildings of the tested type satisfies the demands for the construction of earthquake resistant buildings located in seismic hazard zones with design ground acceleration $BSC_{\mathrm{d}} = Sa_{\mathrm{g}} = 0.30$, where $S = 1.2$—soil factor and $a_{\mathrm{g}} = 0.25$—design ground acceleration for type A ground (CEN 2004). On the basis of test results, it can be also concluded that the range of values of structural behaviour factor q, proposed in Eurocode 8 for confined masonry buildings, is adequate also for AAC masonry buildings. Taking into account the damage limitation requirement, the use of value $q = 2.5$ is recommended. Although the experiments indicated the possibility of using higher values, additional experimental research to study the correlation between the compressive and tensile strength of AAC masonry and influence of confinement on the seismic behaviour of walls and buildings is needed before proposing new values.

Based on the observed storey shear mechanism, a simple model has been proposed to simulate the seismic response of tested buildings, idealised as lumped mass system. In the model, storey resistance curves, calculated by a push-over method and idealised as a tri-linear relationship, represent the skeleton curves of hysteretic behaviour at each mass level. Hysteretic behaviour is simulated by simple rules, defined by experimentally determined damage and energy dissipation based stiffness and strength degradation parameters.

It has been shown that by using this, relatively simple numerical model, good agreement between the experimentally observed and calculated non-linear response of buildings of the tested type can be obtained.

Acknowledgments The research discussed in this article was financed by Xella Porobeton SI, Ltd. from Kisovec, Slovenia, who also provided materials and workmanship for the construction of models. In this regard, the contribution of Mr. Uroš Klemen from Xella Porobeton SI, Ltd. to the success of the project is gratefully acknowledged.

References

Alcocer SM, Arias JG, Flores LE (2004) Some developments on performance based seismic design of masonry structures. In: Fajfar P, Krawinkler H (eds) Performance-based seismic sesign. Concepts and implementation. PEER Report 2004/2005, pp 33–44, Berkeley

Bertero V, Uang CM (1992) Issues and future directions in the use of an energy approach for seismic resistant design of structures. In: Fajfar P, Krawinkler H (eds) Nonlinear seismic analysis and design of reinforced concrete buildings. Elsevier, London, pp 3–22

CEN (2004) Eurocode 8: design of structures for earthquake resistance, Part 1: general rules, seismic actions and rules for buildings. EN 1998-1:2004. CEN, Brussels

Costa AA, Penna A, Magenes G (2011) Seismic performance of autoclaved aerated concrete (AAC) masonry: from experimental testing of the in-plane capacity of walls to building response simulation. J Earthq Eng 15(1):1–31

Earthquake resistant design of load-bearing Ytong structures, Manual (2004) Xella Porobeton SI (in Slovene)

Harris GH, Sabnis GM (1999) Structural modeling and experimental techniques. CRC Press, Boca Raton

Langhaar HL (1951) Dimensional analysis and theory of models. Wiley, New York

Magenes G (2006) Masonry building design in seismic areas: recent experiences and prospects from a European point of view. In: The 1st European conference on earthquake engineering and seismology. CD-ROM, Geneva, Keynote Address K9: paper 4009

Park YJ, Reinhorn AM, Kunnath SK (1987) IDARC: inelastic damage analysis of reinforced concrete frame—shear-wall structures. Tech Rep NCEER-87-0008. National Center for Earthquake Engineering Research, Buffalo

Schöps P, Jäger W (2009) Confined masonry—a chance to improve the load bearing capacity. In: 11th Canadian masonry symposium, CD-ROM, Toronto

Tanner JE, Varela JL, Klingner RE, Brightman MT, Cancino U (2005) Seismic testing of autoclaved aerated concrete shearwalls: a comprehensive review. ACI Struct J 102(3):374–382

Tomaževič M (1978) Improvement of computer program POR. Report ZRMK-IK, Ljubljana (in Slovene)

Tomaževič M, Velechovsky T (1992) Some aspects of testing small-scale masonry building models on simple earthquake simulators. Earth Eng Struct Dyn 21(11):945–963

Tomaževič M, Lutman M (1996) Seismic behavior of masonry walls: modeling of hysteretic rules. J Str Eng ASCE 122(9):1048–1055

Tomaževič M (1999) Earthquake-resistant design of masonry buildings. Imperial College Press, London

Tomaževič M (2007) Damage as a measure for earthquake-resistant design of masonry structures: Slovenian experience. Can J Civ Eng 34(11):1403–1412

Tomaževič M, Weiss P (2010) Displacement capacity of masonry buildings as a basis for the assessment of behavior factor and experimental study. Bull Earthquake Eng 8:1267–1294

Tomaževič M, Gams M (2010) Seismic behavior of Ytong houses: a shaking table study. Research Report ZAG P 0891/08-650-2, Ljubljana

Turnšek V, Čačovič F (1971) Some experimental results on the strength of brick masonry walls. In: Proceedings 2nd international brick-masonry conference. British Ceramic Society, stoke-on-trent, pp 149–156